IEEE Access
Multidisciplinary ⋮ Rapid Review ⋮ Open Access Journal

Received 15 August 2023, accepted 27 August 2023, date of publication 4 September 2023, date of current version 12 September 2023.

Digital Object Identifier 10.1109/ACCESS.2023.3311631

RESEARCH ARTICLE

Exploring the Parametric Effect in Nonlinear Acoustic Waves

MARÍA CAMPO-VALERA[1], ISIDRO VILLÓ-PÉREZ[2], ALEJANDRO FERNÁNDEZ-GARRIDO[1], IGNACIO RODRÍGUEZ-RODRÍGUEZ[3], AND RAFAEL ASOREY-CACHEDA[1], (Member, IEEE)

[1]Department of Information and Communication Technologies, Universidad Politécnica de Cartagena, 30202 Cartagena, Spain
[2]Department of Electronics and Computer Technologies and Projects, Universidad Politécnica de Cartagena, 30202 Cartagena, Spain
[3]Department of Communication Engineering, Universidad de Málaga, 29071 Málaga, Spain

Corresponding author: María Campo-Valera (maria.campo@upct.es)

This work is a result of the ThinkInAzul programme and was supported by Ministerio de Ciencia e Innovación (MICIN) with funding from European Union NextGenerationEU/Plan de Recuperación, Transformación y Resiliencia (PRTR-C17.I1) and by Fundación Séneca with funding from Comunidad Autónoma Regiónde Murcia (CARM). This work was also supported by the grants TED2021-129336B-I00 and PID2020-116329GB-C22 funded by MICIN/Agencia Estatal de Investigación (AEI)/10.13039/501100011033 and by the European Union NextGenerationEU/Plan de Recuperación, Transformación y Resiliencia (PRTR).

ABSTRACT Nonlinear acoustics is a critical area of study with practical applications in fields such as underwater communications, medical imaging, non-destructive testing, and sonar. This paper offers a comprehensive analysis of the Westervelt and Burgers equations, along with their related boundary problems, and investigates the characteristics of parametric generation, thereby making substantial advancements in the theoretical comprehension of nonlinear acoustic waves. Our analysis sheds new light on the dynamics of nonlinear acoustic waves and their behavior in various media, providing valuable insights into the physics of sound propagation. Finally, parametric effects can be intelligently exploited for communication applications. Thus, through the appropriate selection of encodings, it is possible to develop underwater acoustic communication systems with greater directivity and range than classical systems.

INDEX TERMS Nonlinear acoustic, Westervelt equation, Burgers equation, parametric effect, acoustic communication, underwater acoustic, ultrasound, signal processing.

I. INTRODUCTION

Most known acoustic phenomena are associated with linear elastic properties of the medium [1], [2], [3], [4], [5], [6]. The interaction of an acoustic signal with the medium is said to be linear if the response of the medium and the intensity of the output signal vary linearly with the intensity of the input signal. However, when the intensity of the input signal is large, or in the case of materials with special properties, a series of new nonlinear effects appear, such as distortion of the acoustic wave shape due to the propagation velocity of the wave as a function of amplitude, generation of upper harmonics, generation of sum and difference frequencies of the emitted signals, among others. Knowledge of nonlinear effects is important for the development of new applications in high-intensity acoustics, since these effects are increasingly used in nondestructive characterization of materials [7], [8], [9], [10], medical acoustics [11], [12] and underwater acoustics [13], [14], [15], [16], [17], [18], [19], [20], [21], [22].

The problems of nonlinear acoustics has been studied since the 18th century [23]. Several early developments were compiled by Beyer [24] in a collection of reference papers on nonlinear acoustics. Between the 1960s and 1970s, underwater applications of nonlinear acoustics based on the parametric effect technique were investigated in detail, focusing on the development of parametric arrays [25], [26], [27], since their main feature is that they present an extremely narrow directional pattern (their characteristic width is 1° – 3°) for low-frequency acoustic signals. In this sense, the beamwidth of a parametric array is almost constant over a wide frequency band, while the side lobes

The associate editor coordinating the review of this manuscript and approving it for publication was Yougan Chen.

TABLE 1. List of variables.

Variables	Description
x	Spatial coordinate x
t	Time
$f(x)$	A function of x
c_o	Small-signal sound speed
$c(p)$	Local wave velocity
t_{tv}	Vertical tangent time
t_{sh}	Shock time
x_{sh}	Shock distance
p	Absolute pressure
ρ	Absolute mass density
$\vec{u}$	Absolute velocity vector
p_o, ρ_o, $\vec{u}_o$	Equilibrium quantities
p', ρ', $\vec{u}'$	Acoustic quantities
μ	Shear viscosity
μ_b	Bulk viscosity
δ	Diffusivity of sound
B/A	Nonlinear parameter
β	Coefficient of nonlinearity
$\mathcal{P}_o$	Pressure amplitude
k_c	Complex dispersion relation
k_o	Wave number
ω_o	Angular frequency
α_o	Attenuation coefficient
L_a	Absorption length
$\mathcal{L}$	Lagrangian density
τ	Retarded time
I_n	Modified Bessel function of the first kind and order n
Γ	Gol'dberg number
ω_c	Carrier angular frequency
ω_m	Modulating angular frequency
ω_d	Difference frequency

are absent [28]. In the early 1970s, parametric arrays were used in both civilian and military applications, and much research was carried out in this field [29], [30]. Considerable theoretical advances in the understanding of nonlinear acoustic phenomena were also achieved during this period [31], [32], [33], [34], [35], [36]. Thus, authors such as Hamilton and Blackstock [23] and Enflo and Hedberg [37] provided reviews on the theory and some applications of nonlinear acoustics.

Recently, the development of mathematical simulation techniques has led to an increase in attempts to better understand this behavior and thus improve the various existing applications [38], [39], [40], [41], [42], [43].

This paper presents a comprehensive study of nonlinear acoustics, which solves the one-dimensional Westervelt wave equation using the Burgers equation to understand nonlinear wave propagation. This analysis compares linear and nonlinear effects on the frequency spectrum to demonstrate the impact of nonlinearity on the frequency spectrum.

The rest of the paper is organized as follows. Section II primarily focuses on the effects related to nonlinearity, where the authors demonstrate the propagation of Gaussian pulse with initial condition, for linear and nonlinear case. In Section III, the hydrodynamic model is introduced to derive the fundamental equations of sound. The authors analyze the first and second order approximations (linear and nonlinear order) used to obtain the Westervelt and Burgers equations. Section IV presents the development of the one-dimensional Westervelt equation, which leads to the viscous Burgers equation. This model is widely used due to its simplicity in observing the formation of collision singularities within a finite time, which distinguishes nonlinear equations from linear ones. In Section V, various boundary problems with different excitations are studied to demonstrate the spectral evolution over the propagation distance. Section VI discusses the parametric effect and provides an experimental measurements regarding the directivity benefits of this technique, particularly useful for sonar and communication applications [44], [45], [46], [47], [48], [49], [50], [51], as shown in Section VII. Finally, Section VIII presents the concluding remarks.

II. EFFECTS ASSOCIATED WITH NONLINEAR PROPAGATION

To facilitate comprehension and tracking of the work, the authors present Table 1, which describes the list of variables used in this paper.

For simplicity, the one-dimensional case will be discussed. The propagation of waves in the $+x$-direction is governed by the linear wave equation of first order[1]:

$$\frac{\partial p(x,t)}{\partial t} + c_o \frac{\partial p(x,t)}{\partial x} = 0, \tag{1}$$

where c_o is the speed of acoustic wave measured in small amplitude. In a finite medium, the absence of boundary conditions will be considered. The general solution of the first-order wave equation (1) is:

$$p(x,t) = f(x - c_o t), \tag{2}$$

where $f(x)$ is a function given by the initial conditions of the Cauchy problem, $f(x) = p(x,0)$.

Since c_o is a constant, the solution (2) has the property of keeping its shape throughout the propagation. In other words, for each time t the curve $f(x)$ shifts to the right without deformation, an amount $c_o t$. This behavior is characteristic in a linear regime.

However, if the signal's amplitude is not negligible, the linear model is no longer valid. In this case, the nonlinear model will be considered. To describe the nonlinear behavior, the Burgers equation will be taken as a starting point. The Cauchy problem for the Burgers equation is expressed as:

$$\begin{cases} \dfrac{\partial p(x,t)}{\partial t} + c(p)\dfrac{\partial p(x,t)}{\partial x} = 0 & \text{(3a)} \\ p(x,0) = f(x) & \text{(3b)} \end{cases}$$

[1]The one-dimensional linear wave equation of the second order:

$$\frac{\partial^2 p(x,t)}{\partial t^2} - c_o \frac{\partial^2 p(x,t)}{\partial x^2} = 0$$

can be factored by means of the operators:

$$L^+ = \left(\frac{\partial}{\partial t} + c_o \frac{\partial}{\partial x}\right), \quad L^- = \left(\frac{\partial}{\partial t} - c_o \frac{\partial}{\partial x}\right),$$

where the sign $+$ corresponds to waves propagating to the right and the sign $-$ to waves propagating to the left. Thus, the second-order one-dimensional wave equation gives rise to two first-order wave equations.

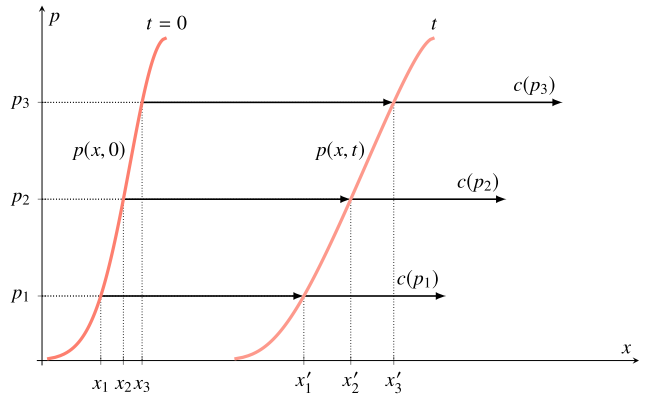

FIGURE 1. Each p_i remains constant moving with a certain speed $c(p_i)$. At the instant t the pressure p_i will have traveled a distance $c(p_i)t$ where $x_i' = x_i + c(p_i)t$.

where $c(p)$ is a given function that depends in turn on the solution itself $p = p(x, t)$.

The mathematical form of the Burgers equation (3a) is observed to be identical to the linear equation (1), with the only difference being that the velocity $c(p)$ is no longer a constant. When the velocity c depends on p, it gives rise to a nonlinear first-order wave equation.

The first consequence of nonlinearity is that the superposition principle is not fulfilled. A second consequence is that the methods used to solve linear differential equations (separation of variables, Laplace transform, Fourier transform, Green function, among others) can not be applied to nonlinear problems.

The Cauchy problem, expressions (3a) to (3b), admits a solution that is known as a solution or Riemann wave and is given by:

$$p(x, t) = f[x - c(p)t] \tag{4}$$

The linear solution (2) and the nonlinear solution (4) have the same shape but very different behaviors. Indeed, the functional dependence of c with p implies that each point of the initial curve $p(x, 0) = f(x)$ will propagate at different speeds. This behavior is illustrated in Figure 1. When the wave has a profile $p(x, 0) = f(x)$ at time $t = 0$, it undergoes changes over time and develops a distinct profile $p(x, t)$ after a certain duration. In this scenario, we are dealing with a local wave velocity $c(p)$.

As a consequence of the above, the wave profile will be deformed until the solution becomes multivalued and, therefore, lacks physical meaning (the solution must be a single-valued function of position). As the wave breaks (*the wave breaking*), a discontinuous solution is considered, which is called a shock wave. The shock wave (*sh*) occurs at a certain position x_{sh} and at a certain instant of time t_{sh} (*the breaking time*). The equation (3a) will only be valid if $t \leq t_{sh}$. For $t > t_{sh}$ the equation (3a) does not adequately describe the physical phenomenon, and it is necessary to review some of the initial approximations and assumptions. Mathematically, the existence of this singularity can be verified in (4) by changing of variable:

$$\xi = x - c(p)\,t \quad \Longrightarrow \quad p(\xi) = f(\xi) \tag{5}$$

$$\frac{\partial p}{\partial t} = \frac{df}{d\xi}\frac{\partial \xi}{\partial t} = -\left(c + t\frac{dc}{dp}\frac{\partial p}{\partial t}\right)\frac{df}{d\xi} \tag{6}$$

$$\frac{\partial p}{\partial x} = \frac{df}{d\xi}\frac{\partial \xi}{\partial x} = \left(1 - t\frac{dc}{dp}\frac{\partial p}{\partial x}\right)\frac{df}{d\xi} \tag{7}$$

Solving for the first derivatives $\partial p/\partial t$ and $\partial p/\partial x$ results in:

$$\frac{\partial p(x, t)}{\partial t} = -\frac{c(p)f'(\xi)}{1 + c'(p)f'(\xi)t} \tag{8}$$

$$\frac{\partial p(x, t)}{\partial x} = \frac{f'(\xi)}{1 + c'(p)f'(\xi)t} \tag{9}$$

where the prime index ($'$) denotes derivatives with respect to their variables. These derivatives diverge giving rise to a vertical tangent (*tv*), if the denominators go to zero at some place or time. This happens if $1 + c'(p)f'(\xi)\,t = 0$. From where:

$$t_{tv} = \frac{-1}{c'(p)f'(\xi)} \tag{10}$$

The smallest value of t_{tv} is what is considered t_{sh}:

$$t_{sh} = \frac{-1}{c'(p)f'_{min}(\xi)}, \tag{11}$$

To illustrate these concepts and make them more specific, Section II-A studies the propagation of a Gaussian pulse.

A. PROPAGATION OF A GAUSSIAN PULSE WITH INITIAL CONDITIONS

Let us consider the Cauchy initial value problem for the Burgers equation whose initial wave profile is a Gaussian pulse of amplitude $\mathcal{P}_o$, and the local wave velocity $c(p)$ is a linear function of p:

$$\begin{cases} \dfrac{\partial p(x, t)}{\partial t} + (c_o + ap)\dfrac{\partial p(x, t)}{\partial x} = 0 \\ p(x, 0) = \mathcal{P}_o e^{-x^2} \end{cases} \tag{12}$$

where $c_o > 0$ and $a \geq 0$ are constants that are assumed to be known.

According to (3a) and (3b) it turns out to be:

$$c(p) = c_o + ap, \quad 0 \leq p \leq \mathcal{P}_o \tag{13}$$

$$f(x) = \mathcal{P}_o e^{-x^2} \tag{14}$$

It can be observed that the local wave velocity $c(p)$ grows from a minimum value c_o (for $p = 0$) to a maximum value $c_o + a\mathcal{P}_o$ (for $p = \mathcal{P}_o$). Next, we will consider the cases, $a = 0$ and $a > 0$.

1) LINEAR CASE, $A = 0$

If $a = 0$, the problem reduces to a linear problem whose solution is given by (2):

$$p(x,t) = f(x - c_o t) = \mathcal{P}_o e^{-(x-c_o t)^2} \tag{15}$$

Since c_o is a constant, the Gaussian wave profile propagates without deformation with velocity c_o as shown in Figure 2.

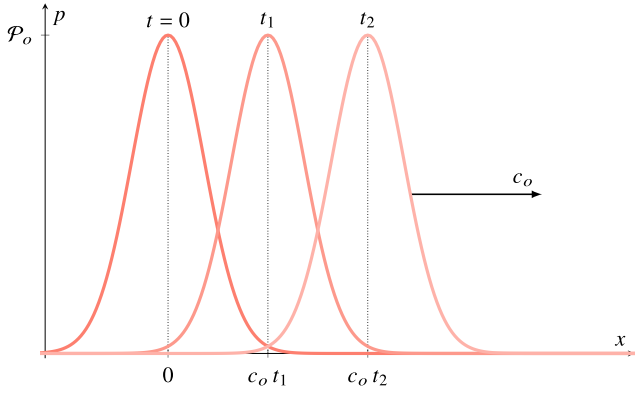

FIGURE 2. Propagation in a linear regime. The pulse propagates without deformation.

2) NONLINEAR CASE, $A > 0$

If $a > 0$, the solution to the initial value problem (12) is a Riemann wave given by (4):

$$\begin{aligned} p(x,t) &= f[x - c(p)t] = \mathcal{P}_o e^{-[x-c(p)t]^2} \\ &= \mathcal{P}_o e^{-[x-(c_o+ap)t]^2} \end{aligned} \tag{16}$$

As the local wave velocity $c(p) = c_o + ap$ grows from c_o to $c_o + a\mathcal{P}_o$ the curve will slope to the right because the points of greatest pressure are also those of higher speed. This behavior is shown in the Figure 3. At a certain point, the curve will tilt to such an extent that it becomes multi-valued, leading to the emergence of a *shock wave* or wave break, as mentioned in the preceding section.

By utilizing the expression (11), we can determine the moment at which the *shock wave* occurs. Nevertheless, in this context, we will approach the problem differently. We begin with the inverse of the function (16), which is:

$$x(p,t) = (c_o + ap)t \pm \sqrt{\ln \frac{\mathcal{P}_o}{p}}, \quad 0 \le p \le \mathcal{P}_o \tag{17}$$

where the sign $+$ corresponds to the right branch and the sign $-$ to the left branch with respect to the maximum of the function. It is evident that the *crash* occurs in the right branch. Therefore, it will be enough to consider only the $+$ sign in the function (17). Using the derivative of the inverse function (a t constant) we obtain:

$$\frac{\partial p(x,t)}{\partial x} = \left[\frac{\partial x(p,t)}{\partial p}\right]^{-1} = \frac{2p\sqrt{\ln \frac{\mathcal{P}_o}{p}}}{2apt\sqrt{\ln \frac{\mathcal{P}_o}{p}} - 1} \tag{18}$$

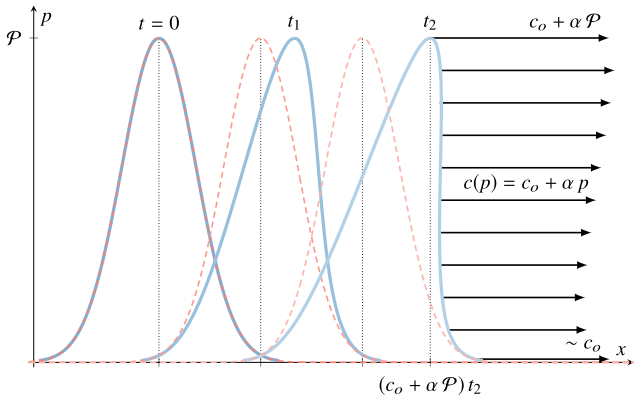

FIGURE 3. Propagation in a nonlinear regime. The pulse deforms due to the local wave velocity $c(p) = c_o + ap$. The red color curve corresponds to the linear regime shown in the (Figure 2).

The collision occurs when the derivative becomes infinite. That is, if:

$$2apt\sqrt{\ln \frac{\mathcal{P}_o}{p}} - 1 = 0 \quad \Rightarrow \quad t(p) = \frac{1}{2ap\sqrt{\ln \frac{\mathcal{P}_o}{p}}} \tag{19}$$

To obtain the pressure and time values where the *shock* occurs (defined as p_{sh} and t_{sh}), the absolute minimum of the function $t(p)$ must be calculated. This calculation can be done by equating the first derivative to zero:

$$\frac{dt(p)}{dp} = \frac{1 - 2\ln \frac{\mathcal{P}_o}{p}}{4p^2 a \left[\ln \frac{\mathcal{P}_o}{p}\right]^{\frac{3}{2}}} = 0 \quad \Longrightarrow \quad 1 - 2\ln \frac{\mathcal{P}_o}{p} = 0 \tag{20}$$

from where,

$$p_{sh} = e^{-\frac{1}{2}}\, \mathcal{P}_o \simeq 0.607\, \mathcal{P}_o \tag{21}$$

substituting (21) in (19) we obtain:

$$t_{sh} = \frac{e^{\frac{1}{2}}}{\sqrt{2}} \frac{1}{a\mathcal{P}_o} \simeq \frac{1.166}{a\mathcal{P}_o} \tag{22}$$

It remains to determine the position where the collision occurs. This position is obtained by substituting the results (21) and (22) into (17):

$$x_{sh} = \frac{1}{\sqrt{2}} \left(2 + e^{\frac{1}{2}} \frac{c_o}{a\mathcal{P}_o}\right) \tag{23}$$

In Figure 4, the wave profile is depicted at the moment of the shock and at a subsequent time. To plot this figure, the following numerical values were taken:

$$\mathcal{P}_o = 1 \text{ MPa}, \quad c_o = 1481.44 \text{ m/s}, \quad a = 6.753 \cdot 10^{-6} \text{ m}^2\text{s/kg}$$

Substituting these values in (21), (22), and (23) we get

$$p_{sh} = 0.607 \text{ MPa}, \quad t_{sh} = 0.173 \text{ s}, \quad \text{y} \quad x_{sh} = 257.167 \text{ m}$$

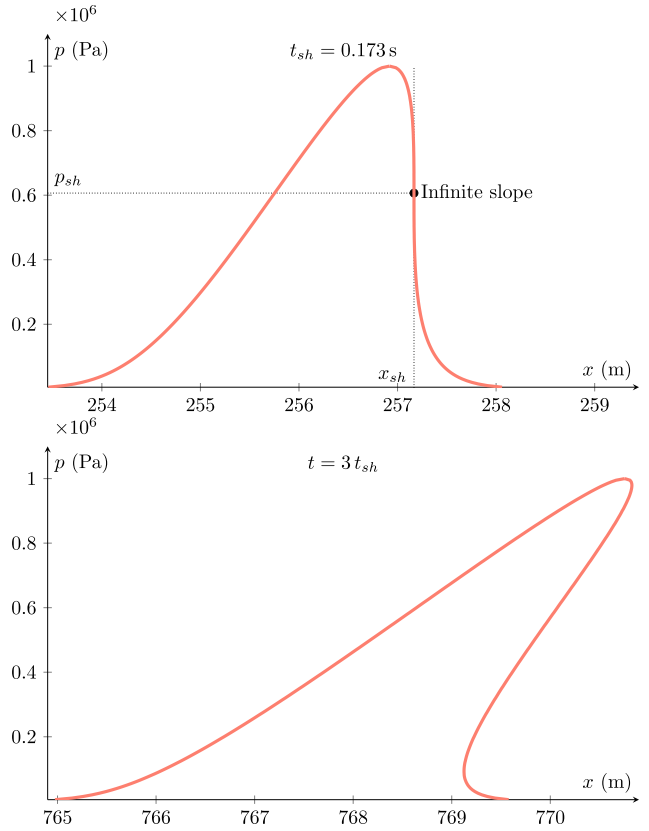

FIGURE 4. For $t > t_{sh}$ the curve becomes so steep that it is multivalued.

It can be observed that, for $t > t_{sh}$ the function is no longer undervalued and the solution is no longer valid. Therefore, the Cauchy problem (12) is physically acceptable only if $t \leq 0.173$ s.

In viscous fluids (dissipative or lossy fluids), the wave can develop a vertical slope but the solution never becomes multivalued. The nonlinear behavior of waves in viscous fluids will be analyzed in the following sections.

III. HYDRODYNAMIC MODEL

The hydrodynamic model is the starting point to derive the fundamental equations of acoustics. Unfortunately, the full set of hydrodynamic equations has not yet been solved, not even in the computational case (due to the large number of required operations and instability problems). Therefore, it is necessary to simplify the model in order to obtain closed analytical or numerical solutions.

Depending on the problem under consideration, several models with different degrees of approximation can be used. Here we will use the Continuity and Navier-Stokes equations, which will be approximated to second order.

In addition, the Westervelt equation is widely used in the field of nonlinear acoustics, and it is obtained from the hydrodynamic model under certain assumptions and approximations. It is important to know these approximations to bound their limits and range of validity.

- Continuity equation: It mathematically states the principle of conservation of mass and in differential form. It is expressed as:

$$\frac{\partial \rho}{\partial t} + \vec{\nabla} \cdot (\rho \vec{u}) = 0, \tag{24}$$

where $\rho = \rho(\vec{r}, t)$ is the mass density and $\vec{u} = \vec{u}(\vec{r}, t)$ the velocity vector associated with the motion of the fluid particles.

- Navier-Stokes equation: It is derived from the law of conservation of momentum or Newton's second law for viscous fluids. In the absence of external forces, the Navier-Stokes equation takes the form:

$$\rho \left[\frac{\partial \vec{u}}{\partial t} + (\vec{u} \cdot \vec{\nabla}) \vec{u} \right] + \vec{\nabla} p = \mu \nabla^2 \vec{u} + \left(\mu_b + \frac{1}{3} \mu \right) \vec{\nabla} (\vec{\nabla} \cdot \vec{u}) \tag{25}$$

where $p = p(\vec{r}, t)$ is the pressure, μ_b the bulk viscosity and μ the shear viscosity. The term $(\vec{u} \cdot \nabla)\vec{u}$ is called the convective or transport acceleration term.

Using the vector identities:

$$\vec{\nabla} \cdot (\rho \vec{u}) = \vec{u} \cdot \vec{\nabla} \rho + \rho \vec{\nabla} \cdot \vec{u} \tag{26}$$

$$(\vec{u} \cdot \vec{\nabla}) \vec{u} = \frac{1}{2} \vec{\nabla} u^2 - \vec{u} \times \left(\vec{\nabla} \times \vec{u} \right) \tag{27}$$

$$\vec{\nabla} (\vec{\nabla} \cdot \vec{u}) = \nabla^2 \vec{u} + \vec{\nabla} \times (\vec{\nabla} \times \vec{u}) \tag{28}$$

where $u^2 = \vec{u} \cdot \vec{u}$. We can write the Continuity equation (24) and the Navier-Stokes equation (25) as:

$$\begin{aligned} &\frac{\partial \rho}{\partial t} + \vec{u} \cdot \vec{\nabla} \rho + \rho \nabla \cdot \vec{u} = 0 \\ &\times \rho \left[\frac{\partial \vec{u}}{\partial t} + \frac{1}{2} \vec{\nabla} u^2 - \vec{u} \times \left(\vec{\nabla} \times \vec{u} \right) \right] + \vec{\nabla} p \\ &= \left(\mu_b + \frac{4}{3} \mu \right) \nabla^2 \vec{u} + \left(\mu_b + \frac{1}{3} \mu \right) \vec{\nabla} \times (\vec{\nabla} \times \vec{u}) \end{aligned} \tag{29}$$

The variables that appear in these equations are absolute amounts of pressure, density, and velocity. Assuming the fluid is initially in equilibrium, the propagation of an acoustic wave will produce a disturbance, a deviation from the values at equilibrium. Thus, absolute quantities can be decomposed as the sum of two terms:

$$\begin{aligned} p(\vec{r}, t) &= p_o + p'(\vec{r}, t) \\ \rho(\vec{r}, t) &= \rho_o + \rho'(\vec{r}, t) \\ \vec{u}(\vec{r}, t) &= \vec{u}_o + \vec{u}'(\vec{r}, t) \end{aligned} \tag{30}$$

The subscript zero denotes values at equilibrium and the prime index denotes disturbed values. For example, p' represents the deviation suffered by the pressure from the equilibrium state p_o, this disturbance is known as acoustic pressure.

A homogeneous medium is assumed, thus ρ_o and p_o are constant (independent of position and time). It is also assumed that the fluid velocity in equilibrium is zero $\vec{u}_o = 0$ and, if edge effects are neglected, it can also

be assumed that the acoustic velocity vector field $\vec{u}'$ is irrotational $\vec{\nabla} \times \vec{u}' = 0$. Under these assumptions, if we substitute (30) in (29) we obtain:

$$\frac{\partial \rho'}{\partial t} + \rho_o \vec{\nabla} \cdot \vec{u}' = -\vec{u}' \cdot \vec{\nabla} \rho' - \rho' \vec{\nabla} \cdot \vec{u}' \tag{31}$$

$$\rho_o \frac{\partial \vec{u}'}{\partial t} + \vec{\nabla} p' = -\rho' \frac{\partial \vec{u}'}{\partial t} - \frac{1}{2} \rho_o \vec{\nabla} u'^2 - \frac{1}{2} \rho' \vec{\nabla} u'^2 + \mu_1 \nabla^2 \vec{u}' \tag{32}$$

To facilitate the notation, we have defined the viscosity term μ_1 as:

$$\mu_1 = \mu_b + \frac{4}{3}\mu \tag{33}$$

It is important to stress that the system of equations (31) and (32) is a system formed by a scalar and a vector equation. Therefore, it is an indeterminate system, as it contains four equations and five unknown variables (p', ρ', u'_x, u'_y, and u'_z). For the system to be complete, it is necessary to add one more equation, this third equation is the equation of state. Assuming barotropic fluids (the pressure depends only on the density), the equation of state (to second-order) takes the form ([52]):

$$\rho' = \frac{p'}{c_o^2} - \frac{1}{\rho_o c_o^4} \frac{B}{2A} p'^2 \tag{34}$$

where c_o is the small-signal sound speed (evaluated at the equilibrium state) and B/A is a dimensionless quantity known as *nonlinear parameter*.

The objective is to solve the system of equations (31), (32) and (34) assuming that the fluctuations are relatively small i.e. p'/p_o, ρ'/ρ, $u'/u_o \ll 1$. This will make it possible to disregard terms from a certain order of accuracy. Using the method introduced by Blackstock [52], the order of a certain term can be classified according to the following criteria:

- First-order terms are those that are linear with respect to the disturbance. For example, first-order terms are all those placed to the left of equality in equations (31) and (32).
- Second-order terms are all quadratic terms that appear in the cross products between disturbed quantities. For example, second-order terms are all those placed to the right of equality in the equations (31) and (32), with the exception of the term $\rho' \vec{\nabla} u'^2$, which is of higher order.
- All the rest are higher order terms.

A. APPROXIMATION OF FIRST ORDER (LINEAR ACOUSTICS)

For signals of small amplitude, the characteristic displacement of the magnitudes of the fluid with respect to their equilibrium values is very small. This condition defines the hypothesis of linear acoustics. Under this hypothesis, with a good degree of approximation, we can neglect in the equations (31), (32), and (34) the terms of order greater than one. Under these conditions, the Continuity equation, Navier-Stokes equation and the equation of state reduce to:

$$\begin{cases} \dfrac{\partial \rho'}{\partial t} + \rho_o \vec{\nabla} \cdot \vec{u}' = 0 & \text{(35a)} \\ \rho_o \dfrac{\partial \vec{u}'}{\partial t} + \vec{\nabla} p' = \mu_1 \nabla^2 \vec{u}' & \text{(35b)} \\ \rho' = \dfrac{p'}{c_o^2} & \text{(35c)} \end{cases}$$

These system of equations is the mathematical basis of linear acoustics propagation in lossy media. The system consists of two coupled differential equations (35a) and (35b), and a third equation (35c) that links them linearly. This allows one of the three variables to be solved to obtain a decoupled equation. For p', we obtain:

$$\nabla^2 p' - \frac{1}{c_o^2} \frac{\partial^2 p'}{\partial t^2} = -\frac{\delta}{c_o^2} \frac{\partial}{\partial t} \left(\nabla^2 p' \right) \tag{36}$$

which is the well known linear wave equation in viscous fluids, and $\delta \equiv \mu_1/\rho_o$ is called the *diffusivity of sound*.

Without loss of generality, the system will be limited to the one-dimensional case, for which the equation (36) takes the form:

$$\frac{\partial^2 p'}{\partial x^2} - \frac{1}{c_o^2} \frac{\partial^2 p'}{\partial t^2} = -\frac{\delta}{c_o^2} \frac{\partial}{\partial t} \left(\frac{\partial^2 p'}{\partial x^2} \right) \tag{37}$$

For plane harmonic waves,

$$p'(x,t) = \mathcal{P}_o e^{j(k_c x - \omega_o t)} \tag{38}$$

It is easy to show that the *complex dispersion relation* takes the form:

$$k_c = \frac{\omega_o}{c_o} \left(1 - j \frac{\omega_o \delta}{c_o^2} \right)^{-\frac{1}{2}} \simeq \simeq \frac{\omega_o}{c_o} \left(1 + j \frac{\delta \omega_o}{2 c_o^2} \right) \equiv k_o + j\alpha_o \tag{39}$$

with $k_o = \omega_o/c_o$ the wave number, and α_o the attenuation coefficient at the frequency ω_o:

$$\alpha_o = \frac{\delta \omega_o^2}{2 c_o^3} \tag{40}$$

The inverse of α_o is called the *absorption length* and is denoted by the symbol L_a, that is:

$$L_a = \frac{1}{\alpha_o} \tag{41}$$

Substituting (39) in (38) and taking the imaginary part, we obtain the form of an attenuated linear wave:

$$p'(x,t) = \mathcal{P}_o e^{-\alpha_o x} \sin \omega_o \left(t - \frac{x}{c_o} \right) \tag{42}$$

It can be observed that, when $x = L_a$, the amplitude of the signal is attenuated by a factor $\mathcal{P}_o/e$. It can also be observed from (40) that the attenuation coefficient α_o depends on the square of the frequency. For this reason, higher frequency waves will dissipate faster than lower frequency waves.

On the other hand, for plane harmonic waves, it is easy to prove that the structure relationship between p' and u' is given by:

$$\frac{p'}{u'} = \rho_o c_o \sqrt{1 + \frac{\delta^2 \omega_o^2}{2c_o^3}} e^{j \tan^{-1}\left(\frac{\delta \omega_o}{2c_o^2}\right)} \tag{43}$$

which is called *complex acoustic impedance*. For lossless media, it reduces to:

$$\frac{p'}{u'} = \rho_o c_o \tag{44}$$

B. APPROXIMATION OF SECOND ORDER (NONLINEAR ACOUSTICS)

In large amplitude signals, the linear model is no longer valid and it will be necessary to consider higher order terms. Most of the applications of interest can be formulated with a good degree of accuracy under a second order approximation.

In the equations (31), (32) and (34), all the terms involved are second order except the term $\rho' \vec{\nabla} u'^2$ which is third order. Thus, for a second order approximation we have:

$$\frac{\partial \rho'}{\partial t} + \rho_o \vec{\nabla} \cdot \vec{u}' = -\vec{u}' \cdot \vec{\nabla} \rho' - \rho' \vec{\nabla} \cdot \vec{u}' \tag{45}$$

$$\rho_o \frac{\partial \vec{u}'}{\partial t} + \vec{\nabla} p' = -\rho' \frac{\partial \vec{u}'}{\partial t} - \frac{1}{2} \rho_o \vec{\nabla} u'^2 + \mu_1 \nabla^2 \vec{u}' \tag{46}$$

Next, it is necessary to make use of the substitution corollary which indicates that any second order relation can be substituted by its first order approximation, since the resulting error is of third order [52]. Thus, we can use the first-order linear model equations (35a), (35b), and (35c) (taking μ_1 equal to zero) to approximate the second-order terms in the equations (45), (46). After some algebra, the result is:

$$\begin{cases} \dfrac{\partial \rho'}{\partial t} + \rho_o \vec{\nabla} \cdot \vec{u}' = \dfrac{1}{\rho_o c_o^4} \dfrac{\partial p'^2}{\partial t} + \dfrac{1}{c_o^2} \dfrac{\partial \mathcal{L}}{\partial t} & \text{(47a)} \\ \rho_o \dfrac{\partial \vec{u}'}{\partial t} + \vec{\nabla} p' = -\dfrac{\delta}{c_o^2} \dfrac{\partial}{\partial t} \left(\vec{\nabla} p' \right) - \vec{\nabla} \mathcal{L} & \text{(47b)} \\ \rho' = \dfrac{p'}{c_o^2} - \dfrac{1}{\rho_o c_o^4} \dfrac{B}{2A} p'^2 & \text{(47c)} \end{cases}$$

where $\mathcal{L}$ is called the second-order *Lagrangian density* and it is defined as:

$$\mathcal{L} \equiv \frac{1}{2} \left(\rho_o u'^2 - \frac{p'^2}{\rho_o c_o^2} \right) \tag{48}$$

According to the linear relationship (44), it can be observed that, for plane harmonic waves in lossless media, $\mathcal{L} = 0$.

The three equations (47a), (47b) and (47c) are the basic equations of second-order nonlinear acoustics in lossy media. As in the linear case, now we remove p' and obtain the wave equation for the acoustic pressure:

$$\nabla^2 p' - \frac{1}{c_o^2} \frac{\partial^2 p'}{\partial t^2} = -\frac{\delta}{c_o^4} \frac{\partial^3 p'}{\partial t^3} - \frac{\beta}{\rho_o c_o^4} \frac{\partial^2 p'^2}{\partial t^2} - \left(\nabla^2 \mathcal{L} + \frac{1}{c_o^2} \frac{\partial^2 \mathcal{L}}{\partial t^2} \right) \tag{49}$$

where β is called the *coefficient of nonlinearity* and it is defined as:

$$\beta = 1 + \frac{B}{2A} \tag{50}$$

IV. WESTERVELT AND BURGERS EQUATION

Westervelt's equation [53] is perhaps the best known equation in the field of nonlinear acoustics, whose study was based on the "scattering of sound by sound". This equation is obtained by making the approximation $\mathcal{L} = 0$ in the wave equation (49). The Lagrangian density $\mathcal{L}$ can be omitted when cumulative nonlinear effects dominate over local nonlinear effects [52], [54]. Making this approximation, the Westervelt equation takes the form:

$$\nabla^2 p' - \frac{1}{c_o^2} \frac{\partial^2 p'}{\partial t^2} = -\frac{\delta}{c_o^4} \frac{\partial^3 p'}{\partial t^3} - \frac{\beta}{\rho_o c_o^4} \frac{\partial^2 p'^2}{\partial t^2} \tag{51}$$

From the one-dimensional form of the Westervelt equation, the Burgers equation is derived [54]:

$$\frac{\partial p'}{\partial x} = \frac{\beta p'}{\rho_o c_o^3} \frac{\partial p'}{\partial \tau} + \frac{\delta}{2c_o^3} \frac{\partial^2 p'}{\partial \tau^2} \tag{52}$$

where $\tau = t - x/c_o$ is the delay. For lossless media ($\delta = 0$), the Burgers equation is known as inviscid Burgers equation. Undoing the change of temporal variable in (52), the inviscid Burgers equation takes the form:

$$\frac{\partial p'}{\partial t} + c(p') \frac{\partial p'}{\partial x} = 0 \tag{53}$$

with

$$c(p') = c_o \left(1 - \frac{\beta p'}{\rho_o c_o^2} \right)^{-1} \simeq c_o + a p' \tag{54}$$

where $a = \beta / \rho_o c_o$. It can be observed that (54) is the local wave velocity that was used in the Cauchy problems (12).

The inviscid Burgers equation is one the most popular nonlinear one dimensional wave equations and is widely used as it is a simple model in which the formation of shock singularities is observed in finite times. The formation of these singularities is one of the phenomena that best distinguishes nonlinear equations from linear ones.

V. BURGERS EQUATION: BOUNDARY VALUE PROBLEMS

Analytical solutions for Burgers equation are well known and documented in the literature. In this section we analyze several boundary value problem for the viscous Burgers equation which will allow us show clearly the parametric effect and its applications to underwater communications.

A. MONO-FREQUENCY HARMONIC EXCITATION: MENDOUSSE SOLUTION

In this section, we consider the boundary value problem for the viscous Burgers equation (52) with a mono-frequency harmonic boundary condition:

$$\begin{cases} \dfrac{\partial p'}{\partial x} = \dfrac{\beta p'}{\rho_o c_o^3}\dfrac{\partial p'}{\partial \tau} + \dfrac{\delta}{2c_o^3}\dfrac{\partial^2 p'}{\partial \tau^2} \\ p'(0,t) = \mathcal{P}_o \sin \omega_o t \end{cases} \tag{55}$$

This problem supports an explicit solution known as the *Mendousse solution* [55], which is shown in equation (56), as shown at the bottom of the page.

This solution is valid $\forall x$, being I_n the modified Bessel function of the first kind and order n and Γ the so-called Gol'dberg number defined as:

$$\Gamma = \frac{L_a}{x_{sh}} = \frac{2\beta \mathcal{P}_o}{\delta \omega_o \rho_o} \tag{57}$$

where L_a is the absorption length given in (41) and x_{sh} the shock distance (distance where the wave will develop a vertical slope) given by:

$$x_{sh} = \frac{\rho_o c_o^3}{\beta \mathcal{P}_o \omega_o} \tag{58}$$

The Mendousse solution (56) is represented in Figure 5 with different observation planes. For this, the following numerical values were taken:

$$c_o = 1481.44 \text{ m/s}, \quad \rho_o = 999.6 \text{ kg/m}^3, \quad \beta = 10,$$
$$\delta = 0.005 \text{ m}^2/\text{s} \quad f_o = 0.1 \text{ MHz}, \quad \mathcal{P}_o = 1 \text{ MPa}$$

From these values we obtain: $x_{sh} = 51.72$ cm, $\alpha_o = 0.30 \text{ m}^{-1}$, $L_a = 3.29$ m, and $\Gamma = 6.37$.

In Figure 5, it can be observed that at $x = 0$ the Mendousse solution reproduces the initial wave profile given by the boundary condition in (55). At $x = 0.5\, x_{sh}$, the wave undergoes deformation as anticipated compared to the linear solution. At $x = x_{sh}$, the shock wave occurs, resulting in the development of vertical slopes in the curve. Between $x = x_{sh}$ and $x = 3x_{sh}$, the wave progressively transforms, eventually taking on a sawtooth shape. Beyond $x = 3x_{sh}$, the wave continues to evolve as a sawtooth, gradually attenuating due to dissipation. Finally, for $x \gg L_a$, the wave gradually returns to its initial profile, albeit with a significantly reduced amplitude.

This figure illustrates the distortion and spectral change of a nonlinear wave. Despite what it may seem, these effects are not a disadvantage, but quite the opposite. The spectral richness of nonlinear waves can be exploited in a variety of practical applications, particularly in the field of acoustic communications.

B. BI-FREQUENCY HARMONIC EXCITATION: LARDNER SOLUTION

Let us consider the boundary problem for the viscous Burgers equation (52) with a bi-frequency harmonic boundary condition:

$$\begin{cases} \dfrac{\partial p'}{\partial x} = \dfrac{\beta p'}{\rho_o c_o^3}\dfrac{\partial p'}{\partial \tau} + \dfrac{\delta}{2c_o^3}\dfrac{\partial^2 p'}{\partial \tau^2} \\ p'(0,t) = \mathcal{P}_a \sin \omega_a t + \mathcal{P}_b \sin \omega_b t \end{cases} \tag{59}$$

ω_a and ω_b must be positive integer multiples of a certain frequency ω_o, that is:

$$\omega_a = a\omega_o, \quad \omega_b = b\omega_o \tag{60}$$

where a and b are two natural numbers. Moreover, for any $\mathcal{P}_a$ and $\mathcal{P}_b$ it is always possible to choose a value $\mathcal{P}_o$ such that:

$$\mathcal{P}_a = A\mathcal{P}_o \quad \mathcal{P}_b = B\mathcal{P}_o \tag{61}$$

with A and B being real numbers.

This boundary problem supports the solution of expression (62), as shown at the bottom of the page, known as the Lardner solution [37], [56], which is the bi-frequency extension of the Mendousse solution of expression (56).

The Figure 6 shows the Lardner's solution to the boundary problem of expression (59) with the following numerical values:

$$c_o = 1481.44 \text{ m/s}, \quad \rho_o = 999.6 \text{ kg/m}^3, \quad \beta = 3.5,$$
$$\delta = 0.0016 \text{ m}^2/\text{s}, \quad f_o = 0.1 \text{ MHz}, \quad \mathcal{P}_o = 2 \text{ MPa},$$
$$\omega_a = 9\omega_o, \quad \omega_b = 7\omega_o, \quad A = B = 1$$

The red curve presents the linear solution:

$$p'(x,t) = \mathcal{P}_a e^{-\alpha_a t} \sin \omega_a \left(t - \frac{x}{c_o}\right) + \mathcal{P}_b e^{-\alpha_b t} \sin \omega_b \left(t - \frac{x}{c_o}\right) \tag{63}$$

$$p'(x,t) = -\mathcal{P}_o \frac{4\,\Gamma^{-1} \sum_{n=-\infty}^{\infty} n\,(-1)^n I_n \dfrac{\Gamma}{2} e^{-n^2\alpha_o x} \sin\left(n\,\omega_o \left(t - \frac{x}{c_o}\right)\right)}{I_o \dfrac{\Gamma}{2} + 2 \sum_{n=-\infty}^{\infty} (-1)^n I_n \dfrac{\Gamma}{2} e^{-n^2\alpha_o x} \cos\left(n\,\omega_o \left(t - \frac{x}{c_o}\right)\right)} \tag{56}$$

$$p'(x,t) = -\mathcal{P}_o \frac{2\Gamma^{-1} \sum_{l=-\infty}^{\infty} \sum_{m=-\infty}^{\infty} (la+mb)(-1)^{l+m} I_l\left(\frac{A}{2a}\Gamma\right) I_m\left(\frac{B}{2b}\Gamma\right) e^{-(la+mb)^2\alpha_o x} \sin(l\omega_a + m\omega_b)\left(t - \frac{x}{c_o}\right)}{\sum_{l=-\infty}^{\infty} \sum_{m=-\infty}^{\infty} (-1)^{l+m} I_l\left(\frac{A}{2a}\Gamma\right) I_m\left(\frac{B}{2b}\Gamma\right) e^{-(la+mb)^2\alpha_o x} \cos(l\omega_a + m\omega_b)\left(t - \frac{x}{c_o}\right)} \tag{62}$$

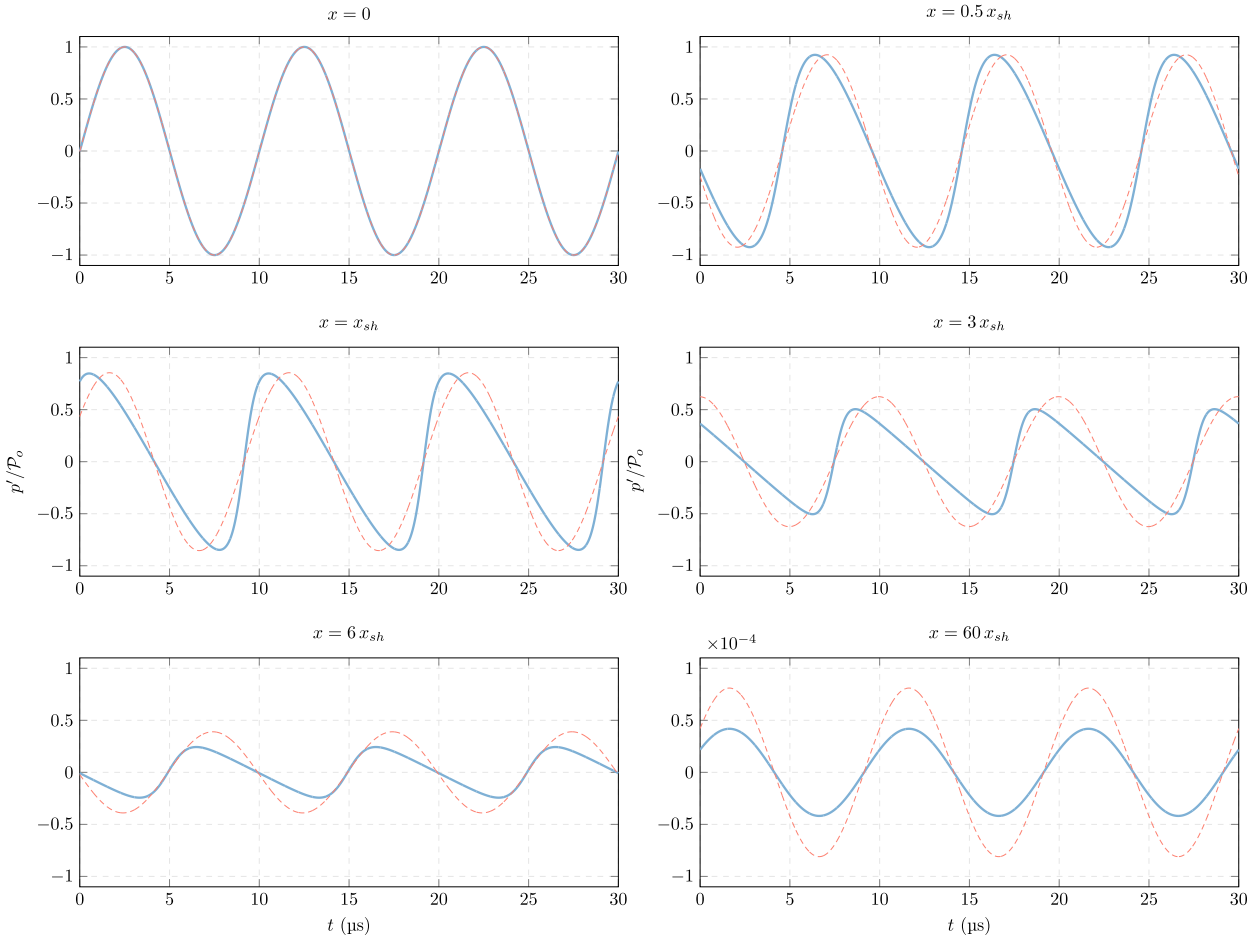

FIGURE 5. Mendousse solution in different observation planes. The red curve shows the linear solution of expression (42).

where α_a and α_b are the attenuation coefficients at the frequencies ω_a and ω_b, respectively.

In the Figure 6, it can be observed that during propagation frequencies are generated that are linear combinations of the primary frequencies $\omega_a = 9\omega_o$ and $\omega_b = 7\omega_o$. It is important to note that for $x > 1\ m$ the dominant frequency is the difference frequency $(9 - 7 = 2)$ and the higher order harmonics have been strongly attenuated. With $x = 3\ m$, the signal is basically a mono-frequency signal oscillating at the difference frequency $2\omega_o$. The signal maintains this shape for a large distance until it finally transfers its energy to the fundamental mode ω_o. This evolution is shown in the Figure 7.

C. MODULATED EXCITATION IN A VISCOUS MEDIUM

As a last example, we consider the contour problem for the viscous Burgers equation whose boundary condition is a sinusoidal function of amplitude A_c and frequency ω_c (carrier frequency) modulated in amplitude by a function $E(t)$:

$$\begin{cases} \dfrac{\partial p'}{\partial x} = \dfrac{\beta p'}{\rho_o c_o^3}\dfrac{\partial p'}{\partial \tau} + \dfrac{\delta}{2c_o^3}\dfrac{\partial^2 p'}{\partial \tau^2} \\ p'(0,t) = A_c E(t)\sin\omega_c t \end{cases} \tag{64}$$

In order to obtain an analytical solution, the simplest case of all possible cases will be taken as modulating function, a cosine function of frequency $\omega_m (< \omega_c)$. Thus, the boundary condition in (64) takes the form:

$$\begin{aligned} p'(0,t) &= A_c \cos(\omega_m t)\sin(\omega_c t) \\ &= \frac{A_c}{2}\sin(\omega_c + \omega_m)t + \frac{A_c}{2}\sin(\omega_c - \omega_m)t \\ &= \mathcal{P}_o \sin\omega_a t + \mathcal{P}_o \sin\omega_b t \end{aligned} \tag{65}$$

with $\mathcal{P}_o = 1/2A_c$, $\omega_a = \omega_c + \omega_m$ and $\omega_b = \omega_c - \omega_m$. The problem is reduced to a bi-frequency boundary condition as discussed in the previous section. In order to use Lardner's solution (62), ω_a and ω_b are required to be natural multiples of a certain frequency ω_o. Consequently:

$$\begin{aligned} \omega_c + \omega_m &= a\omega_o \\ \omega_c - \omega_m &= b\omega_o \end{aligned} \tag{66}$$

Solving for ω_c and ω_m from the system of equations (66), we have:

$$\omega_c = \frac{a+b}{2}\omega_o \tag{67}$$

$$\omega_m = \frac{a-b}{2}\omega_o \tag{68}$$

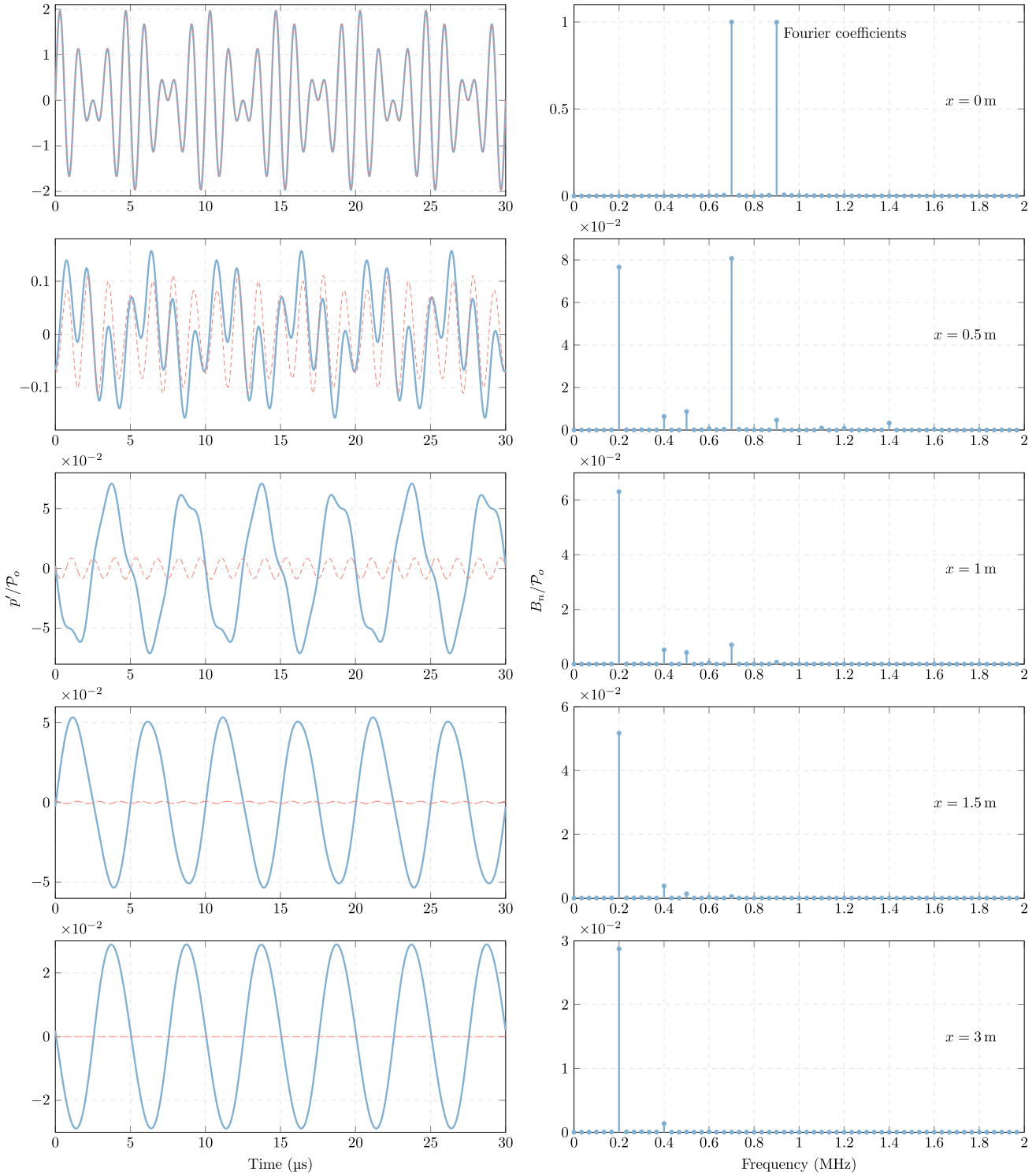

FIGURE 6. Lardner's solution with $\omega_a = 9\,\omega_o$, and $\omega_b = 7\,\omega_o$.

The expression (68) shows that the difference frequency is equal to twice the modulating frequency. This is:

$$\omega_a - \omega_b = (a - b)\omega_o = 2\omega_m \tag{69}$$

As a numerical example, the following modulated signal is considered:

$$p'(0, t) = A_c \cos(\omega_m t) \sin(\omega_c t)$$
$$A_c = 4\ \mathrm{MPa}, \quad f_m = 50\ \mathrm{kHz}, \quad f_c = 650\ \mathrm{kHz}$$

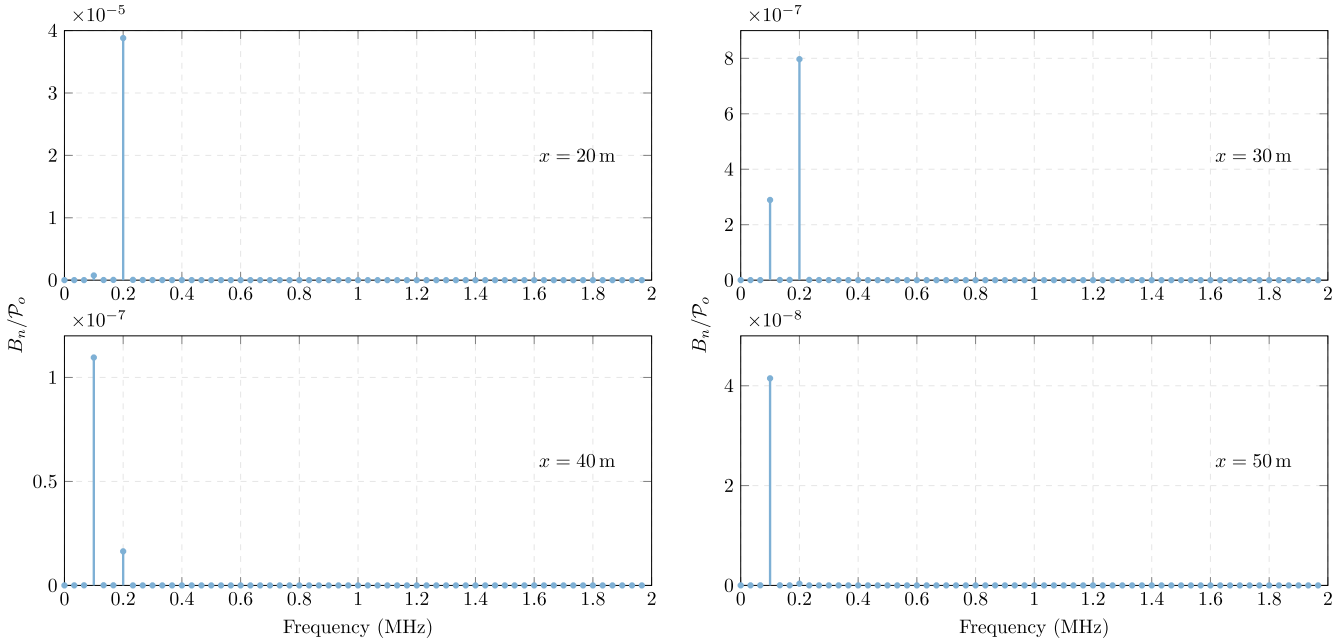

FIGURE 7. At large distances from the boundary, all the energy of the bi-frequency signal is transferred to the fundamental mode ω_o.

From expressions (67) and (68), it is straightforward to show that with the problem is reduced to a bi-frequency excitation with:

$$p\prime(0,t) = \mathcal{P}_o \sin(\omega_a t) + \mathcal{P}_o \sin(\omega_b t)$$
$$\mathcal{P}_o = 2\text{MPa}, \quad f_o = 100\text{kHz} \quad \omega_a = 7\omega_o, \quad \omega_b = 6\omega_o$$

The Figure 8 presents the evolution of the modulated signal in a medium defined by the following values:

$$c_o = 1481.44 \text{ m/s}, \quad \rho_o = 999.6 \text{ kg /m}^3,$$
$$\beta = 3.5, \quad \delta = 0.0016 \text{ m}^2\text{/s}$$

Figure 8 shows that for $x > 3$ m the dominant frequency is the difference frequency $\omega_d = \omega_a - \omega_b = (7-6)\omega_o$. As expected, according to expression (69), the difference frequency is twice the modulating frequency $\omega_d = 2\omega_m$ ($2 \cdot 50$ kHz $= 100$ kHz).

VI. PARAMETRIC EFFECT

The solution to the boundary problem (59) reveals that when two nonlinear harmonic waves with frequencies ω_a and ω_b propagate in the same direction, they mutually interact due to nonlinearity. This interaction gives rise to secondary waves with frequencies that are linear combinations of the sum and difference of the primary frequencies. Additionally, the dissipative properties of the medium cause higher frequency waves to attenuate and eventually vanish over long propagation distances exceeding the absorption length. Consequently, the wave with a frequency difference $\omega_d \equiv \omega_a - \omega_b$ propagates the farthest distance. This phenomenon is referred to as the *parametric effect*, and the wave with the frequency difference ω_d is known as the *parametric signal*.

Hence, when the primary signals consist of two pure tones with frequencies ω_a and ω_b, the resulting parametric signal manifests as a single-component wave. This particular manifestation of the parametric effect is referred to as the *dual parametric effect*. Figure 9 depicts the evolution of the dual signal over the propagation distance for two tones with frequencies $\omega_a/2\pi = 2.3$ MHz and $\omega_b/2\pi = 2$ MHz. Notably, higher frequencies are swiftly absorbed by the medium, resulting in a mono-frequency signal oscillating at the parametric frequency of 0.3 MHz for $x > 20$ cm. The figure was generated using Lardner's solution (62), where $\mathcal{P}_a = \mathcal{P}_b = 1$ MPa and the provided medium parameters:

$$c_o = 1481.44 \text{ m/s}, \quad \rho_o = 999.6 \text{ kg/m}^3,$$
$$\beta = 10, \quad \delta = 0.0016 \text{ m}^2\text{/s}$$

Another method of generating parametric signals is by using a broadband primary signal, in which case an infinite number of frequencies interact to generate a broadband parametric signal. In this case, the parametric effect is called *broadband parametric effect*. This would be the case for a generic boundary condition like the one discussed in the problem (64):

$$p'(0,t) = A_c E(t) \sin \omega_c t \tag{70}$$

where ω_c is the carrier frequency and the modulated amplitude $E(t)$ can be any function that varies slowly compared to $\sin \omega_c t$.

It is commonly understood that generating directional beams for high frequencies is relatively easier compared to low frequencies, as the latter often exhibit more omnidirectional behavior. Nevertheless, one notable characteristic

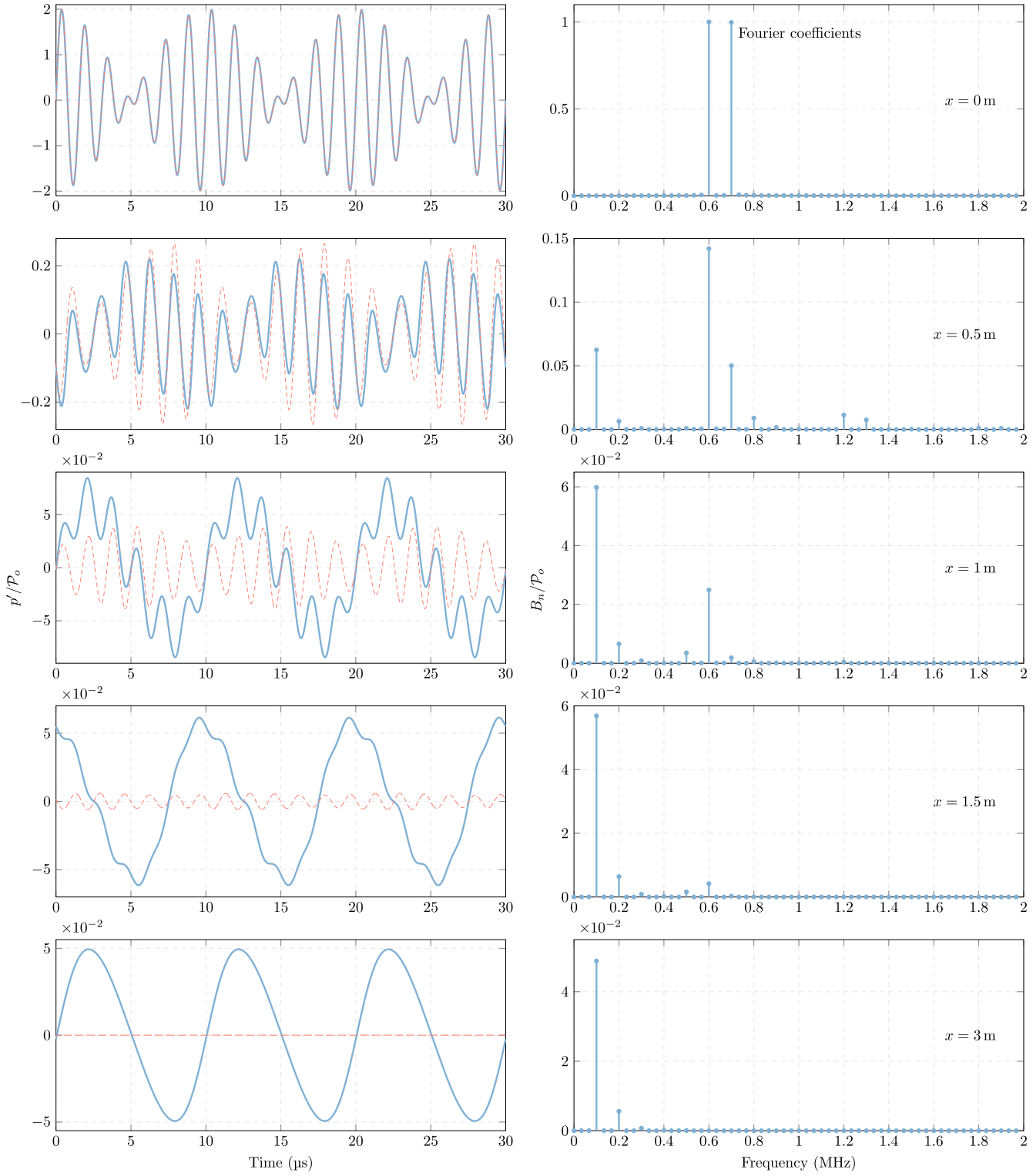

FIGURE 8. Lardner's solution for a modulated signal with $\omega_m = 50\,\mathrm{kHz}$ and $\omega_c = 650\,\mathrm{kHz}$. The red curve shows the linear solution.

of the parametric effect is that low frequencies, when generated through parametric means, display a relatively narrow directivity similar to that of the primary beam. This can be seen in Figure 10.

Figure 10 illustrates the contrasting theoretical directivity achieved through linear and parametric approaches. Notably, the figure highlights the directivity patterns of traditional communication systems (operating within the linear

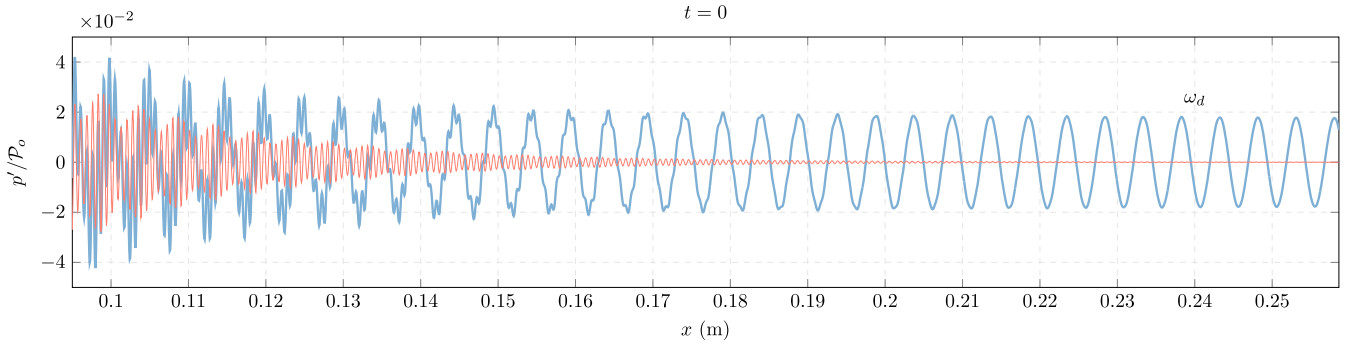

FIGURE 9. Dual parametric effect along the propagation distance (the x axis has been taken on a logarithmic scale from $x = 7$ cm to $x = 25$ cm). The red and blue curves show the linear and nonlinear solution, respectively.

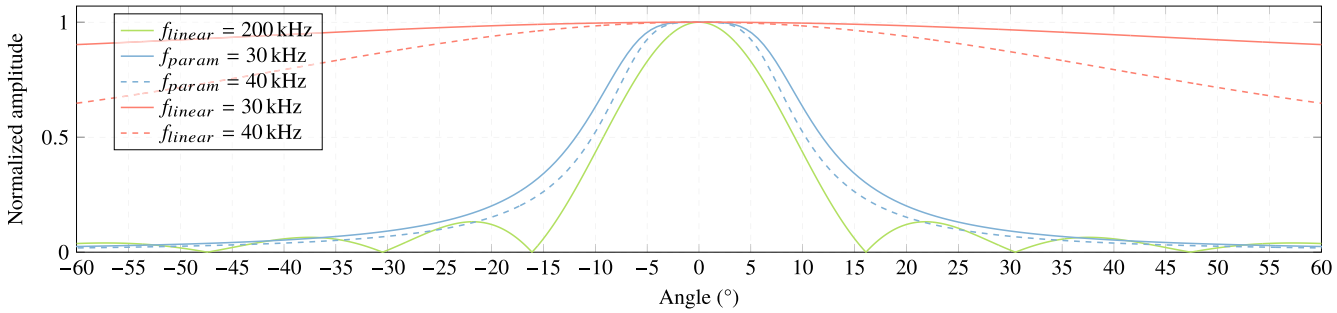

FIGURE 10. Theoretical comparison of directivity between a linear and a nonlinear system.

acoustic realm) at lower frequencies, showcasing their tendency towards omnidirectional radiation (as depicted by the red curves). These patterns exhibit an approximate beamwidth spanning over ±60°. Conversely, the Figure 10 also showcases the directivity patterns of parametric communication systems (pertaining to nonlinear acoustic systems), which demonstrate a remarkable enhancement in radiated beam concentration, with a remarkably narrow span of ±2° (as represented by the blue curves). Comparing the directivity of the parametric system (blue curves) with the linear directivity of a high-frequency scenario (visualized by the green curve) solidifies one of the core attributes of parametric generation. Specifically, it exemplifies the capability of parametric systems to attain a highly directional radiation pattern at lower frequencies, akin to the directional patterns achieved at higher frequencies. This comparison serves to underscore the distinctive characteristic of parametric generation, a capacity to imbue low-frequency radiation patterns with a level of directionality typically associated with higher frequency domains.

An experimental result of the directivity measurement is studied and will be discussed in Section VI-A.

A. EXPERIMENTAL STUDY

Airmar P19 plane transducer is used, with an emission sensitivity of 167 dB re µPa/V @ 1 m at the resonance frequency of 200 kHz and the Reson TC4040 hydrophone.

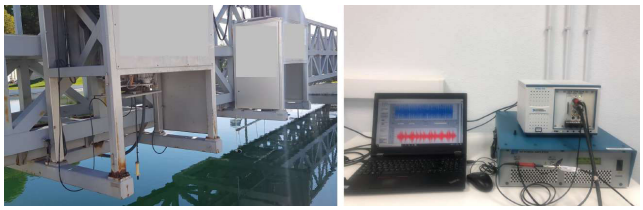

FIGURE 11. Experimental setup.

The measurements were performed in a 10 m deep, 20 m diameter truncated cone-shaped raft with SMARLOGY positioning system, X-axis servo motor BMH1003P32F2A, Y-axis servo motor BMH1003P32F2A.

Figure 11 shows that the equipment used was the NI PXIe 5433 function generator, which is connected to the PC and uses LabVIEW to send the signal to the input of the E&I 1040L RF amplifier, to increase the amplitude of the signal, and through its output to the transducer.

The measurement is evaluated by a sine modulated signal with a carrier frequency of 200 kHz corresponding to the resonance frequency of the Airmar P19 transducer and a modulating frequency of 15 kHz with a duration of 1 ms, obtaining a parametric frequency of 30 kHz. The signal was emitted at a distance of 1 m.

Figure 12 presents the analysis of the linear signal; red curve (high frequency – primary beam) and the signal generated through the parametric effect; blue curve

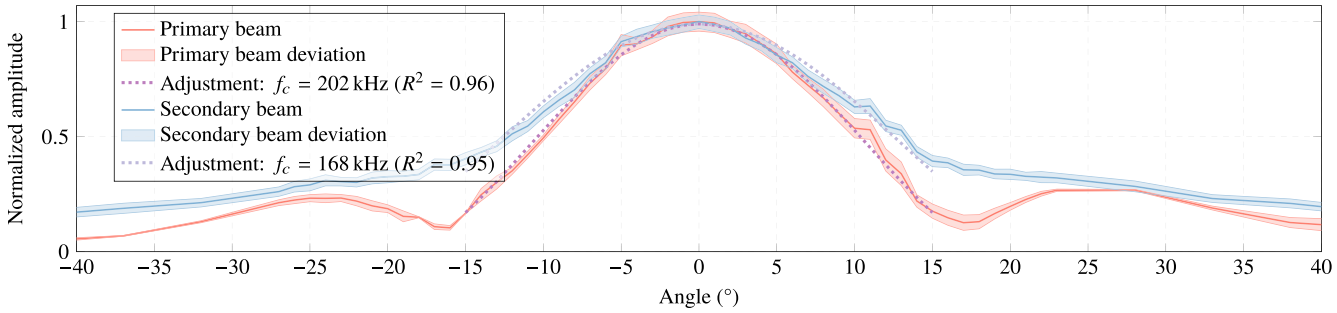

FIGURE 12. Experimental directivity for a 30 kHz parametric sine. Primary beam ±6°, secondary beam ±9° at −3 dB.

(low frequency – secondary beam). Using the minimization of the mean square deviation of the experimental data, they are fitted to the model of the expression (71) of the flat piston, since for the primary beam, the directivity of the main lobe is given through that expression and as the directivity of the secondary beam tends to be similar to that of the primary, then it is appropriate to use this expression as a model for both beams. Starting from expression (71) [57], where J_1 is the first order Bessel function, k is the wavenumber, and r is the piston radius. The adjustment is made taking the transducer radius of 1.65 cm and varying the frequency, a fit with an equivalent frequency for each beam is obtained.

$$D(\theta, \varphi) = \left(\frac{2 \cdot J_1(k \cdot r \cdot \sin\theta)}{k \cdot r \cdot \sin\theta} \right)^2 \tag{71}$$

It can be observed that the directivities are similar despite the spectral differences. A beamwidth of ±6° is obtained for the primary beam and ±9° for the secondary beam. In addition, it can be observed that one of the characteristics of parametric generation is that the sidelobes are mostly null or minimal, as they are for these results.

VII. APPLICATIONS TO UNDERWATER COMMUNICATION

The parametric effect described in Section VI can be effectively utilized in communication applications. To this end, we propose a modulation technique for underwater acoustic communications based on the concatenation of several broadband sine-sweep type signals. In this modulation, the bit '1' is defined by an upward sine-sweep as a modulated signal ($E_{uss}(t)$, ω_{m1} to ω_{m2}, expression (72)), and the bit '0' is defined by a downward sine-sweep ($E_{dss}(t)$, ω_{m2} to ω_{m1}, expression (73)). Fig. 13 illustrates examples of modulated signals for bits '1' and '0' for better visual comprehension. Nevertheless, these signals are transmitted concatenated to form the desired message:

$$E_{uss}(t) = \sin\left[\left(\frac{\omega_{m1} - \omega_{m2}}{\tau_{ss}} t + \omega_{m1} \right) t \right], 0 \le t \le \tau_{ss}, \tag{72}$$

$$E_{dss}(t) = \sin\left[\left(\frac{\omega_{m2} - \omega_{m1}}{\tau_{ss}} (t - \tau_{ss}) + \omega_{m1} \right) (t - \tau_{ss}) \right], \quad 0 \le t \le \tau_{ss}, \tag{73}$$

where τ_{ss} is the bit duration.

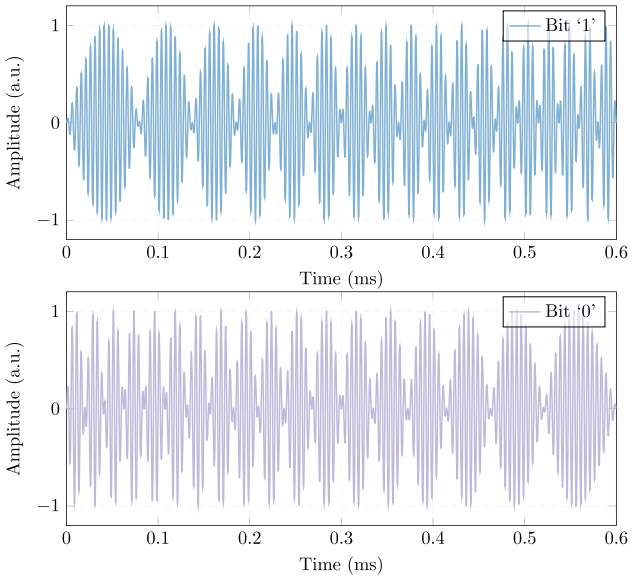

FIGURE 13. Modulated sine-sweep signal at the transmitter.

In the experiments, the sine-sweep envelope for a bit '1' ranged from 5 kHz to 15 kHz, and for a bit '0' ranged from 15 kHz to 5 kHz. Both signals have a duration of $\tau_{ss} = 0.6$ ms, modulated with a sine of frequency carrier $f_c = 200$ kHz. This produces a parametric signal according to the analytical at the receiver similar to the one in the example of Fig. 14. This is the combination of harmonic signals with variable frequency and increasing amplitude as a function of the modulating frequency.

A. SIGNAL PROCESSING

The amplitude of the low-frequency signal due to the parametric effect is lower than the emitted signal, making it difficult to detect, or distinguish from background noise. To demonstrate this empirically, an encoding consisting of a 16-bit string as follows ("0110111101101011") was sent at an emitter-receiver distance of 42 cm. The transmitting and receiving system operates at a sampling frequency of 20 MHz and the bits are emitted continuously.

A good way to check the occurrence of the parametric effect is to analyze it by means of the cross-correlation

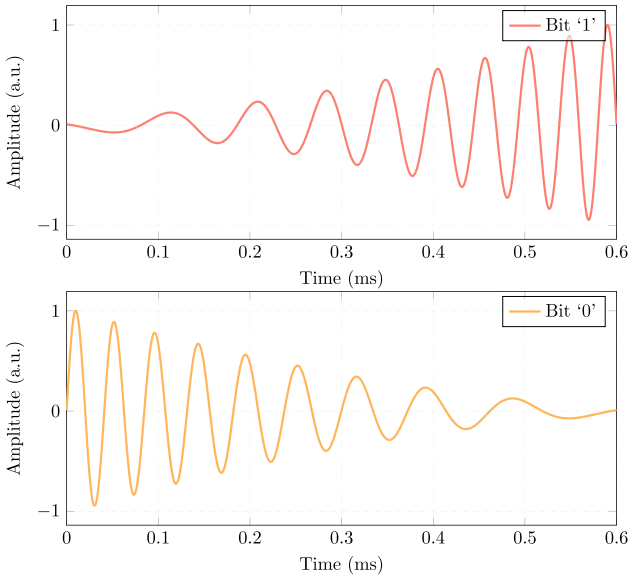

FIGURE 14. Parametric sine-sweep signal at the receiver.

method [58]. It consists of correlating a filter with an impulse response matching the searched signal with the recorded signal. Thus, if a coincidence occurs a peak will appear. In this case, the recorded signal was correlated with parametric bit signals '1' and '0' [18].

Figure 15 illustrates the received signal and the corresponding correlation for both '1' and '0' bits. It clearly demonstrates the distinguishability between the two bits and the ease of detection achieved through this parametric effect. Moreover, upon receiving the message, only receivers familiar with the bit coding can successfully decode it, thereby facilitating the design of more secure underwater communication systems.

B. DISCUSSION

The exploration of parametric acoustic sources traces back to Westervelt, whose theory hinges on the concept of *sound by sound* scattering. Through his research, it was deduced that these parametric sources yield finely focused beams at lower frequencies, boasting minimal side lobes. This impressive outcome is achieved with a compact array of transducers.

For the realm of high-performance underwater acoustic communications, the prerequisites are broad bandwidths to facilitate high data rates and a slender beam profile to mitigate the repercussions of multipath reflections. These demands

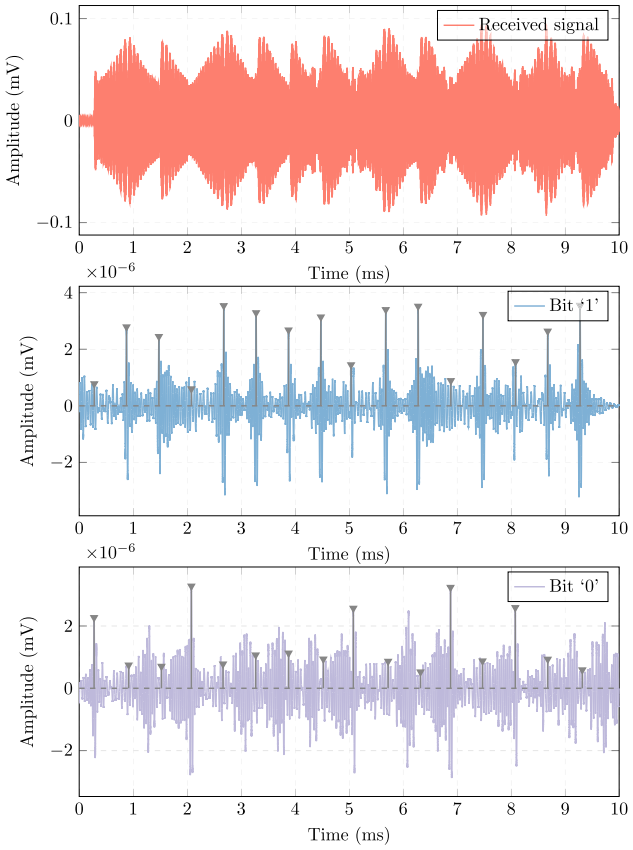

FIGURE 15. Received signal (top), the cross-correlation between the received signal and the expected parametric signal for bit '1' (middle), and the cross-correlation between the received signal and the expected parametric signal for bit '0' (bottom).

find a harmonious solution in parametric acoustic arrays, which can be seamlessly integrated with various existing modulation techniques to yield robust system performance. A concrete illustration of this synergy is showcased in Table 2, where diverse communication systems tailored for seabed penetration and object detection are delineated. Moreover, the advantage of cultivating a narrow, directive beamwidth transcends mere technical merits. It bears the potential to elevate the information-handling capacity of a network, allowing for targeted message dissemination to specific nodes devoid of interception risks. This facet gains heightened significance within the military domain, as it paves the way for covert communication strategies.

The findings underscore the viability of employing parametric sine-sweep modulation as a compelling

TABLE 2. Commercial parametric systems.

System	Modulation	f_c (kHz)	f_d (kHz)	Directivity f_d (°)	Source level ($dB\ re\ a\ \mu Pa\ m$)	Penetration capacity (m)	Depth range (m)
SES 2000 smart [46]	Ricker	90 - 110	5 -15	±2.5°	236	Up to 20	< 0.5 - 100
Topas P18 [59]	Chirp, Ricker	15 - 21	0.5 - 6	±4.5°	4 kHz =∼ 209	> 200	< 20 - 11000
BII - 7543 [60]	Ricker, PSK, FSK, Pulse	180 - 210	2 - 20	±8°	10 kHz => 199	> 20	Max. 300
SeaKing SBP [61]	Sine-type	200	20	±4°	-	-	Up to 400

alternative for nonlinear underwater acoustic communications. This modulation technique emerges as highly promising, primarily attributed to its capacity to generate a substantial bit correlation. This advantageous attribute is largely attributed to the extensive frequency bandwidth harnessed by the modulation process.

VIII. CONCLUSION

This paper presented a comprehensive study of the main equations for nonlinear waves, specifically focusing on the Westervelt and Burgers equations derived from the hydrodynamic model of continuity, as well as the Euler equation. We explored both linear and nonlinear acoustic approximations, including first and second-order effects, and investigated various boundary problems involving mono-frequency, bi-frequency, and modulated harmonic excitation in a viscous medium.

An important aspect discussed in this study is the parametric effect, that arises from nonlinear acoustics and can be achieved through modulated signals. It is important to highlight the significance of this technique in underwater communications and sonar applications, attributing it to the high directivity of the low frequency obtained in the experiments around $\pm 9°$. Additionally, it can be observed a decrease in sidelobes, further validating the potential utility of the parametric effect.

Furthermore, the experimental results aligned with theoretical predictions. This contributes to a better understanding of nonlinear acoustics and reinforces the feasibility and effectiveness of employing parametric signals in practical applications.

Overall, this study sheds light on the behavior of nonlinear waves in the context of acoustic phenomena and provides valuable insights into the potential applications and benefits of the parametric effect in underwater communications and sonar systems.

ACKNOWLEDGMENT

María Campo-Valera is grateful for postdoctoral program Margarita Salas—Spanish Ministry of Universities (funded by European Union NextGenerationEU). Ignacio Rodríguez-Rodríguez would like to thank Plan Andaluz de Investigación, Desarrollo e Innovación (PAIDI), Junta de Andalucía, Spain.

REFERENCES

[1] I. Felis-Enguix, J. Otero-Vega, M. Campo-Valera, I. Villó-Pérez, and J. L. Gómez-Tornero, "Practical aspects of acoustic leaky-wave antennas applied to underwater direction finding," in *Proc. 7th Int. Electron. Conf. Sensors Appl.*, vol. 2, pp. 1–8 and 93, Nov. 2020.

[2] M. R. Zarastvand, M. Ghassabi, and R. Talebitooti, "Acoustic insulation characteristics of shell structures: A review," *Arch. Comput. Methods Eng.*, vol. 28, no. 2, pp. 505–523, Mar. 2021.

[3] M. R. Zarastvand, M. H. Asadijafari, and R. Talebitooti, "Acoustic wave transmission characteristics of stiffened composite shell systems with double curvature," *Compos. Struct.*, vol. 292, Jul. 2022, Art. no. 115688.

[4] H. Seilsepour, M. Zarastvand, and R. Talebitooti, "Acoustic insulation characteristics of sandwich composite shell systems with double curvature: The effect of nature of viscoelastic core," *J. Vibrat. Control*, vol. 29, nos. 5–6, pp. 1076–1090, Mar. 2023.

[5] D. Pardo-Quiles, I. Rodríguez-Rodríguez, J.-V. Rodríguez, M. Campo-Valera, and L. Juan-Llácer, "Analyzing multiple acoustic diffraction over a wide barrier using equivalent knife-edge geometries and Babinet's principle (L)," *J. Acoust. Soc. Amer.*, vol. 153, no. 4, p. 1974, Apr. 2023.

[6] A. López-Segovia, I. Rodríguez-Rodríguez, J.-V. Rodríguez, L. Juan-Llácer, M. Campo-Valera, and W. L. Woo, "Exploring the validity of plane and spherical millimeter-wave incidences for multiple-diffraction calculations in wireless communication systems," *Electronics*, vol. 12, no. 9, p. 2020, Apr. 2023.

[7] Y. Zheng, R. G. Maev, and I. Y. Solodov, "Review/sythèse nonlinear acoustic applications for material characterization: A review," *Can. J. Phys.*, vol. 77, no. 12, pp. 927–967, Mar. 2000.

[8] D. Donskoy, A. Sutin, and A. Ekimov, "Nonlinear acoustic interaction on contact interfaces and its use for nondestructive testing," *NDT E Int.*, vol. 34, no. 4, pp. 231–238, Jun. 2001.

[9] N. Gao, Z. Zhang, J. Deng, X. Guo, B. Cheng, and H. Hou, "Acoustic metamaterials for noise reduction: A review," *Adv. Mater. Technol.*, vol. 7, no. 6, Jan. 2022, Art. no. 2100698.

[10] B. Hu, X. Fang, L. Cheng, J. Wen, and D. Yu, "Attenuation of impact waves in a nonlinear acoustic metamaterial beam," *Nonlinear Dyn.*, vol. 111, pp. 15801–15816, Jul. 2023.

[11] F. A. Duck, "Nonlinear acoustics in diagnostic ultrasound," *Ultrasound Med. Biol.*, vol. 28, no. 1, pp. 1–18, Jan. 2002.

[12] O. V. Rudenko, "Nonlinear acoustics in medicine: A review," *Phys. Wave Phenomena*, vol. 30, no. 2, pp. 73–85, Jun. 2022.

[13] M. Campo-Valera, M. Ardid-Ramírez, D. Diego-Tortosa, I. Felis-Enguix, and J. A. Martínez-Mora, "Estudio del efecto paramétrico en agua con aplicación a un calibrador acústico para detección de neutrinos," in *Proc. 48th Congreso Español de Acústica*, 2017, pp. 1466–1472.

[14] M. Ardid, M. Campo-Valera, D. Tortosa, I. Felis, C. Llorens, and J. Martínez-Mora, "Underwater communication using acoustic parametric arrays," in *Proc. 4th Int. Electron. Conf. Sensors Appl.*, Nov. 2017, pp. 1–7.

[15] M. Campo-Valera, M. Ardid, D. Tortosa, I. Felis, J. Martínez-Mora, C. Llorens, and P. Cervantes, "Acoustic parametric signal generation for underwater communication," *Sensors*, vol. 18, no. 7, p. 2149, Jul. 2018.

[16] A. Zhao, Y. Cheng, T. An, and J. Hui, "Covert underwater acoustic communication system using parametric array," *Mar. Technol. Soc. J.*, vol. 53, no. 1, pp. 20–26, Jan. 2019.

[17] S. Tang, G. Zhu, J. Yin, X. Zhang, and X. Han, "A modulation method of parametric array for underwater acoustic communication," *Appl. Acoust.*, vol. 145, pp. 305–313, Feb. 2019.

[18] M. Campo-Valera, I. Felis-Enguix, and I. Villó-Pérez, "Signal processing for parametric acoustic sources applied to underwater communication," *Sensors*, vol. 20, no. 20, p. 5878, Oct. 2020.

[19] J. An, H. Ra, C. Youn, and K. Kim, "Experimental results of underwater acoustic communication with nonlinear frequency modulation waveform," *Sensors*, vol. 21, no. 21, p. 7194, Oct. 2021.

[20] M. Campo-Valera, R. Asorey-Cacheda, I. Rodríguez-Rodríguez, and I. Villó-Pérez, "Characterization of a piezoelectric acoustic sensor fabricated for low-frequency applications: A comparative study of three methods," *Sensors*, vol. 23, no. 5, p. 2742, Mar. 2023.

[21] M. Campo-Valera, I. Rodríguez-Rodríguez, and J.-V. Rodríguez-Rodríguez, *Conceptos Básicos de la Ciencia del Sonido En El Mar*. Málaga, Spain: UMA Editorial, 2023.

[22] M. Campo-Valera, I. Rodríguez-Rodríguez, J.-V. Rodríguez, and L.-J. Herrera-Fernández, "Proof of concept of the use of the parametric effect in two media with application to underwater acoustic communications," *Electronics*, vol. 12, no. 16, p. 3459, Aug. 2023.

[23] M. F. Hamilton and D. T. Blackstock, *Nonlinear Acoustics*, 1st ed. San Diego, CA, USA: Academic, 1998.

[24] R. T. Beyer, *Nonlinear Acoustics in Fluids*, vol. 18. New York, NY, USA: Van Nostrand Reinhold, 1984.

[25] P. J. Westervelt, "Parametric end-fire array," *J. Acoust. Soc. Amer.*, vol. 32, pp. 934–935, Jul. 1960.

[26] R. T. Beyer, "Parameter of nonlinearity in fluids," *J. Acoust. Soc. Amer.*, vol. 32, no. 6, pp. 719–721, Jun. 1960.

[27] P. J. Westervelt, "Parametric acoustic array," *J. Acoust. Soc. Amer.*, vol. 35, no. 4, pp. 535–537, Apr. 1963.

[28] I. B. Esipov, S. P. Tarasov, V. A. Voronin, O. A. Popov, B. Enflo, C. M. Hedberg, and L. Kari, "Parametric array signal dispersion in shallow water," in *Proc. AIP Conf.*, 2008, pp. 393–396.

[29] H. O. Berktay and D. J. Leahy, "Farfield performance of parametric transmitters," *J. Acoust. Soc. Amer.*, vol. 55, no. 3, pp. 539–546, Mar. 1974.

[30] M. B. Moffett and R. H. Mellen, "Model for parametric acoustic sources," *J. Acoust. Soc. Amer.*, vol. 61, no. 2, pp. 325–337, Feb. 1977.
[31] L. K. Zarembo and V. A. Krasil'nikov, *Introduction in Nonlinear Acoustics*. Nauka, Moscow (in Rusian), 1966.
[32] E. Zabolotskaya and R. V. Khokhlov, "Quasi-plane waves, in the nonlinear acoustics of confined beams," *Sov. Phys. Acoust.*, vol. 15, pp. 35–40, 1969.
[33] R. T. Beyer, *Nonlinear acoustics*. USA: U.S. Department of Defense, Department of the Navy, Naval Sea Systems Command, 1974.
[34] C. W. Turner, "Theoretical foundations of nonlinear acoustics," *Electron. Power*, vol. 24, no. 3, pp. 232, Mar. 1978.
[35] N. Bakhvalov, Y. M. Zhileikin, and E. Zabolotskaya, *Nonlinear Theory of Sound Beams*. College Park, MD, USA: American Institute of Physics, 1987.
[36] M. Yoneyama, J.-I. Fujimoto, Y. Kawamo, and S. Sasabe, "The audio spotlight: An application of nonlinear interaction of sound waves to a new type of loudspeaker design," *J. Acoust. Soc. Amer.*, vol. 73, no. 5, pp. 1532–1536, May 1983.
[37] B. O. Enflo and C. M. Hedberg, "Physical theory of nonlinear acoustics," *Theory of Nonlinear Acoustics in Fluids*. New York, NY, USA: Kluwer, 2002, pp. 1–289.
[38] C. Campos-Pozuelo, B. Dubus, and J. A. Gallego-Juárez, "Finite-element analysis of the nonlinear propagation of high-intensity acoustic waves," *J. Acoust. Soc. Amer.*, vol. 106, no. 1, pp. 91–101, Jul. 1999.
[39] S. González-García, I. Villó-Pérez, R. Martín-Gómez, and B. García-Olmedo, "BiPML: A PML to match waves in bianisotropic media," *Microw. Opt. Technol. Lett.*, vol. 20, no. 1, pp. 44–48, Jan. 1999.
[40] M. Hajihasani, Y. Farjami, S. Gharibzadeh, and J. Tavakkoli, "A novel numerical solution to the diffraction term in the KZK nonlinear wave equation," in *Proc. 38th Annu. Symp. Ultrason. Ind. Assoc. (UIA)*, 2009, pp. 1–9.
[41] H. Li, J. Ma, J. Zhu, and B. Chen, "Numerical and experimental studies on inclined incidence parametric sound propagation," *Shock Vibrat.*, vol. 2019, pp. 1–10, Nov. 2019.
[42] B. Kaltenbacher and V. Nikolić, "Parabolic approximation of quasilinear wave equations with applications in nonlinear acoustics," *SIAM J. Math. Anal.*, vol. 54, no. 2, pp. 1593–1622, Apr. 2022.
[43] I. Villó-Pérez, P.-M. Alcover-Garau, M. Campo-Valera, and R. Toledo-Moreo, "A novel 1D-FDTD scheme to solve the nonlinear second-order thermoviscous hydrodynamic model," *Commun. Nonlinear Sci. Numer. Simul.*, vol. 118, Apr. 2023, Art. no. 107015.
[44] S. W. Li, "Simulation of the acoustic field of broadband parametric sonar," in *Proc. Int. Conf. Electr., Autom. Mech. Eng.*, 2015, pp. 690–693.
[45] T. Shengyu, Z. Guangping, Z. Xiao, Y. Jingwei, G. Longxiang, and S. Wei, "Under-ice underwater acoustic communication based on direct sequence spread spectrum system with parametric emission," in *Proc. IEEE Int. Conf. Signal Process., Commun. Comput. (ICSPCC)*, Aug. 2016, pp. 1–4.
[46] TI GmbH, *Smart SES-2000, Parametric Sub-Bottom Profiler*, Innomar, Rostock, Germany, 2000.
[47] L. Kopp, D. Cano, E. Dubois, L. Wang, B. Smith, and R. F. W. Coates, "Potential performance of parametric communications," *IEEE J. Ocean. Eng.*, vol. 25, no. 3, pp. 282–295, Jul. 2000.
[48] M. Campo-Valera and I. Felis-Enguix, "Técnicas de modulación para las comunicaciones acústicas no lineales," in *Proc. 4th Jornadas JAAS Acstica Audio y Sonido*. Ingeniería de Sonido—UNTREF Universidad Nacional de Tres de Febrero, 2018, pp. 1–223.
[49] Y. Cheng, A. Zhao, J. Hui, T. An, and B. Zhou, "Parametric underwater transmission based on pattern time delay shift coding system," *Math. Problems Eng.*, vol. 2018, pp. 1–7, Dec. 2018.
[50] M. Campo-Valera and I. Felis, "Underwater acoustic communication for the marine environment's monitoring," in *Proc. 6th Int. Electron. Conf. Sensors Appl.*, Nov. 2019, p. 51.
[51] M. Campo-Valera, I. Felis-Enguix, and I. Villó-Pérez, "Técnica de modulación obtenida a partir del efecto paramétrico: Aplicación a sistemas acústicos submarinos de comunicaciones," *Revista de acústica*, vol. 51, no. 3, pp. 24–29, 2020.
[52] D. Blackstock, "Approximate equations governing finite-amplitud sound in thermoviscous fluids," Gen. Dyn., GD/E Rep. GD-1463-52, 1963.
[53] P. J. Westervelt, "Scattering of sound by sound," *J. Acoust. Soc. Amer.*, vol. 29, no. 2, pp. 199–203, Feb. 1957.
[54] M. F. Hamilton and D. T. Blackstock, *Nonlinear Acoustics*, vol. 427. San Diego, CA, USA: Academic Press, 1998.
[55] J. S. Mendousse, "Nonlinear dissipative distortion of progressive sound waves at moderate amplitudes," *J. Acoust. Soc. Amer.*, vol. 25, no. 1, pp. 51–54, Jan. 1953.
[56] R. W. Lardner, "Acoustic saturation and the conversion efficiency of the parametric array," *J. Sound Vibrat.*, vol. 82, no. 4, pp. 473–487, Jun. 1982.
[57] L. E. Kinsler, A. R. Frey, A. B. Coppens, and J. V. Sanders, *Fundamentals of Acoustics*, L. E. Kinsler, Ed. Los Angeles, CA, USA: Univ. de California, 1999.
[58] S. Adriân-Martínez, M. Bou-Cabo, I. Felis, C. D. Llorens, J. A. Martínez-Mora, M. Saldaña, and M. Ardid, "Acoustic signal detection through the cross-correlation method in experiments with different signal to noise ratio and reverberation conditions," in *Ad-hoc Networks and Wireless*. Berlin, Germany: Springer, 2015, pp. 66–79.
[59] *Parametric Sub-Bottom Profiler TOPAS PS 18*, Kongsberg, Kongsberg, Norway, Jul. 2019.
[60] *BII-7543 2019*, Benthowave Instrum. Inc., Acoust. Transducer Syst., Collingwood, ON, Canada, 2019. [Online]. Available: https://www.benthowave.com/contact/default.html
[61] *Seaking SBP-Perfilador Paramétrico Del Subsuelo*, Mar. Vis. S.L., Málaga, Spain. [Online]. Available: https://marinevision.es/

MARÍA CAMPO-VALERA was born in Santa Marta, Colombia, in 1984. She received the B.Sc. degree in sound engineering from San Buenaventura University, Bogotá, Colombia, in 2009, the M.Sc. degree in acoustic engineering from Universitat Politécnica de Valäncia (UPV), Spain, in 2016, and the Ph.D. degree from Universidad Politécnica de Cartagena (UPCT), Spain, in 2020. In January 2021, she was a Postdoctoral Researcher with the Group of Electromagnetism Applied to Telecommunications (GEAT), UPCT, working on the development of educational initiatives for the manufacture of low-cost leaky-wave antennas. In 2021, she was a Visiting Researcher with Escuela Naval de Cadetes Almirante Padilla (ENAP), Cartagena de Indias, Colombia. In January 2022, she joined the University of Málaga, Spain, as a Postdoctoral Researcher with the Communications Engineering Department. She was awarded the competitive two-year grant, named Margarita Salas. Her current research interests include signal processing, sensor design, nonlinear acoustic, and underwater acoustic communications and antennas.

ISIDRO VILLÓ-PÉREZ was born in Caravaca de la Cruz, Murcia, Spain, in March 17, 1969. He received the B.Sc. degree and the Ph.D. degree (cum laude) in physics from the University of Granada, Granada, Spain, in 1993 and 1998, respectively. In 1999, he received the grant from the Spanish Government to research with the Bariloche Atomic Center. Since 2003, he has been an Associate Professor (Profesor Titular) with Universidad Politécnica de Cartagena, Cartagena, Spain. His research interests include nonlinear science and numerical simulation, nanophysics, and plasmonics.

ALEJANDRO FERNÁNDEZ-GARRIDO was born in Linares, Spain, in 1995. He received the degree in telecommunication technology engineering with double mention in sound and image and telecommunication systems from Universidad de Jaén (UJA), Spain, in 2020. He is currently pursuing the master's degree in telecommunication engineering with Universidad de Málaga (UMA), and he is also pursuing the Ph.D. degree in information and communication technologies with Universidad Politécnica de Cartagena (UPCT). His Ph.D. degree is about underwater acoustic communications trying to solve the problems of nonlinear acoustics in the marine environment and acoustic leaky-waves antennas.

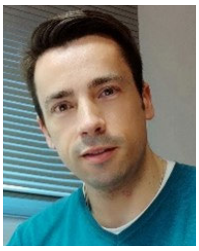

IGNACIO RODRÍGUEZ-RODRÍGUEZ was born in Murcia, Spain, in 1980. He received the technical industrial engineering and superior industrial engineering degrees from Universidad Politécnica de Cartagena (UPCT), Spain, in 2001 and 2004, respectively, and the Ph.D. degree in computer science from Universidad de Murcia (UMU), Spain. In 2015, he joined the Department of Information and Communications Engineering, UMU. He currently works on a postdoctoral contract with the Telecommunications School, University of Mílaga, Spain. His research interests include the application of machine learning to biomedical signals, having works in other fields, such as radio wave diffraction.

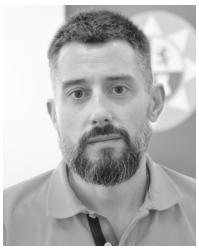

RAFAEL ASOREY-CACHEDA (Member, IEEE) received the M.Sc. degree in telecommunication engineering, major in telematics, and the Ph.D. degree (cum laude) in telecommunication engineering from Universidade de Vigo, Spain, in 2006 and 2009, respectively. He was a Researcher with the Information Technologies Group, Universidade de Vigo, until 2009. From 2008 and 2009, he was a Research and Development Manager of Optare Solutions, a Spanish telecommunications company. He was a Visiting Scholar with New Mexico State University, USA, from 2007 to 2011, and Universidad Politécnica de Cartagena, Spain, in 2011 and 2015. From 2009 and 2012, he held an Ángeles Alvari no position with Xunta de Galicia, Spain. From 2012 to 2018, he was an Associate Professor with Centro Universitario de la Defensa en la Escuela Naval Militar, Universidade de Vigo. He is currently an Associate Professor with Universidad Politécnica de Cartagena. He is the author or coauthor of more than 70 journal and conference papers, mainly in the fields of switching, wireless networking, and content distribution. His research interests include content distribution, high-performance switching, peer-to-peer networking, wireless networks, and nano-networks. He received the Best Master Thesis Award for the M.Sc. degree and the Best Ph.D. Thesis Award for the Ph.D. degree.